Thermo-optic coefficient and nonlinear refractive index of silicon oxynitride waveguides

A. Trenti, M. Borghi, S. Biasi, M. Ghulinyan, F. Ramiro-Manzano, G. Pucker, and L. Pavesi
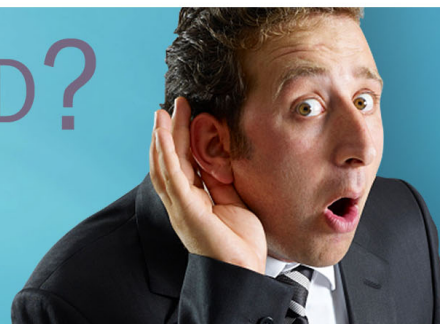
Thermo-optic coefficient and nonlinear refractive index of silicon oxynitride waveguides

A. Trenti,[1,a] M. Borghi,[1,b] S. Biasi,[1] M. Ghulinyan,[2] F. Ramiro-Manzano,[1,3] G. Pucker,[2] and L. Pavesi[1]

[1]*Department of Physics, NanoScience Laboratory, University of Trento, I-38123 Povo, Italy*
[2]*Centre for Materials and Microsystems, Fondazione Bruno Kessler, I-38123 Povo, Italy*
[3]*Instituto de Tecnología Química (CSIC-UPV), Av. de los Naranjos, 46022 Valencia, Spain*

Integrated waveguiding devices based on silicon oxynitride (SiON) are appealing for their relatively high refractive index contrast and broadband transparency. The lack of two photon absorption at telecom wavelengths and the possibility to fabricate low loss waveguides make SiON an ideal platform for on-chip nonlinear optics and for the realization of reconfigurable integrated quantum lightwave circuits. Despite this, very few studies on its linear and nonlinear optical properties have been reported so far. In this work, we measured the thermo-optic coefficient dn/dT and the nonlinear refractive index n_2 of relatively high ($n \sim 1.83$ at a wavelength of 1.55 μm) refractive index SiON by using racetrack resonators. These parameters have been determined to be $\frac{dn}{dT} = (1.84 \pm 0.17) \times 10^{-5} \, \text{K}^{-1}$ and $n_2 = (7 \pm 1) \times 10^{-16} \, \text{cm}^2\text{W}^{-1}$. *© 2018 Author(s).*
All article content, except where otherwise noted, is licensed under a Creative Commons Attribution (CC BY) license (http://creativecommons.org/licenses/by/4.0/).
https://doi.org/10.1063/1.5018016

I. INTRODUCTION

Quantum information science is rapidly developing relying on generation of quantum states of light via emission from quantum dots,[1] colour centres[2] or via frequency conversion mechanisms exploiting material nonlinearities.[3] Silicon photonics is one of the most promising technological platforms for the development of chip-scale densely-integrated quantum devices.[4,5]

Different types of material nonlinearities in Si enable frequency conversion via $\chi^{(3)}$[6] and $\chi^{(2)}$,[7] while its thermo-optical coefficient dn/dT allows for efficient tuning of interference in complex photonic devices.[8] Nonetheless, important free-carrier and two photon absorption issues, as well as the band-to-band absorption below $\sim 1 \mu$m of wavelength, limit the use of Si in several applications.[9,10] The quest for Si-based transparent dielectrics has led to intense studies of alternative materials such as silicon nitride (Si_3N_4),[11] doped silica oxides[12] or oxynitrides.[13] These materials typically possess $\chi^{(3)}$ optical nonlinearities[14] and dn/dT[15,16] from one (nitrides) to two orders (silica) of magnitude lower than those of silicon. Due to the relatively low refractive indices, thicker guiding components are required when these materials are used. High optical quality Si_3N_4 offers the best modal confinement, but may accumulate undesired stress at thicknesses over 200 nm, requiring thus specific design and processing solutions.[17,18]

Here, we report on the study of linear (thermo-optic) and nonlinear $\chi^{(3)}$ optical properties of relatively high ($n \sim 1.83$ at a wavelength of 1.55 μm) refractive index SiON. The detailed characterization, performed on a SiON resonator, revealed a thermo-optic coefficient close to the one of Si_3N_4, and a nonlinear refractive index which is nearly three times the one of SiO_2. In the meanwhile, this material can be grown to relatively high thicknesses ($> 1 \mu m$), offering thus an alternative to the Si_3N_4 platform for the design of nonlinear and quantum optical integrated photonic circuits.

---

[a]Electronic mail: alessandro.trenti@unitn.it

[b]Alessandro Trenti and Massimo Borghi contribute equally to this work.

II. DEVICE FABRICATION AND EXPERIMENTAL SETUP

The device under test is an integrated racetrack resonator in the All-Pass filter configuration.[19] A sketch of the top-view of the device is reported in Fig. 1(a).

The fabrication starts with a deposition of a silicon oxynitride film on top of a 5 μm thermal SiO_2 grown on 6-inch Si wafers. The 600 nm thick SiON layer was grown from a mixture of silane (SiH_4, 50 sccm), ammonia (NH_3, 65 sccm) and nitrous oxide (N_2O, 100 sccm) gases using a parallel-plate plasma enhanced chemical vapour deposition (PECVD) chamber at 3 00 °C. The devices were patterned using an *i*-line optical lithography and defined via dry reactive-ion etching followed by 1.5 h annealing in an N_2 atmosphere at 975 °C to densify (−8 %) the guiding material and to release the excess H_2. Following the work of Bossi et al.,[20] from the refractive index at a wavelength of 850 nm $n_{SiON} = (1.839 \pm 0.001)$, we estimate a Si_3N_4 molar fraction of $(73 \pm 2)\%$, and a SiO_2 molar fraction of $(27 \pm 2)\%$.

The racetrack resonator has a cross section of $1.2 \times 0.55\ \mu m^2$ and bending radius of $R = 50\ \mu m$, while the coupling with the bus waveguide is realized by means of a straight section of length $L = 20\ \mu m$ and a coupling gap of 1.05 μm. The waveguides are single mode for both Transverse Electric (TE) and Transverse Magnetic (TM) polarization at the probe wavelength around 1550 nm. The mode is confined between the lower thermal oxide cladding and the upper one, constituted by a double stack of 400 nm Borophosphosilicate glass (BPSG) and a 2 μm thick PECVD SiO_x layer. The cross-section of the device is reported in Fig. 1(b).

Three separate experimental setups have been used to investigate the device.

The thermo-optic coefficient is determined by using a standard, thermally controlled, passive characterization waveguide setup. We used a C-band tunable Continuous Wave laser (CW), fiber coupled to a polarization controller, which is butt-coupled to the waveguides by means of tapered lensed fibers using a piezoelectric positioning stage. The coupling losses have been estimated with the cut-back technique, which results (6 ± 0.5) dB, equally divided between input and output. With the same technique, the propagation losses have been measured to be (2.0 ± 0.5) dB/cm for both TE and TM polarization at 1550 nm.

As it is possible to see from Fig. 1(c), the device is placed in thermal contact with a Peltier cell, whose temperature can be set in the range of 25-75 °C, with an accuracy of ± 1 °C. The output power is monitored using a germanium photodetector. The laser wavelength is scanned
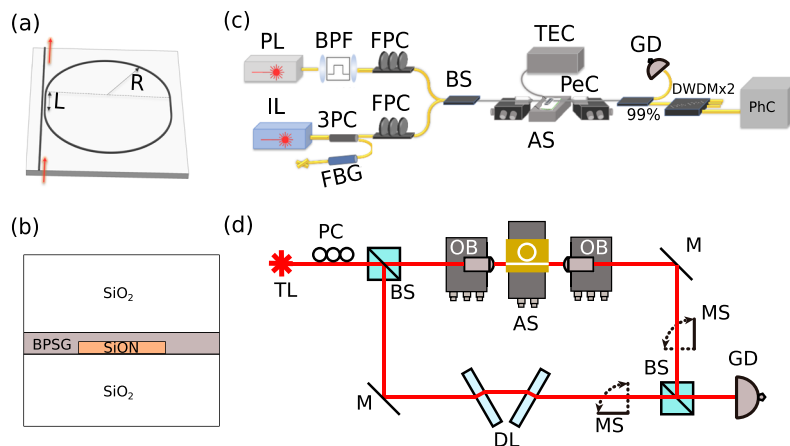
FIG. 1. (a) Top-view of the side-coupled racetrack resonator ($R = 50\ \mu m$ and $L = 20\ \mu m$). The coupling gap is 1.05 μm. (b) Device cross-section. The waveguide cross section is $1.2 \times 0.55\ \mu m^2$. BPSG: Borophosphosilicate glass. (c) Sketch of the experimental set-up used for the thermo-optic and n_2 SiON coefficients. PL: Pump Laser, IL: Idler Laser, BPF: Band-pass Filter, FPC: Fiber Polarization Controller, FBG: Fiber Bragg Grating, 3PC: Three Port Circulator, BS: Beam-splitter, TEC: Temperature Controller, PeC: Peltier Cell, AS: Alignment Stage, GD: Germanium Detector, DWDM: Dense Wavelength Division Multiplexing, PhC: Photon Counter. (d) Sketch of the interferometric experimental set-up for the intensity/phase measurement of the racetrack transmittance as a function of the wavelength. TL: Tunable Laser, OB: Objective, DL: Delay Line, MS: Movable Shutter, M: Mirror.

over the linewidth of the resonator at different fixed temperatures, in order to track the resonance wavelength.

The experimental set-up used to determine the n_2 coefficient makes use of an additional CW tunable laser, called "idler" hereafter, which is combined to the pump laser and injected to the input port of the resonator to stimulate the Four Wave Mixing (FWM) process (see Fig. 1(c)). The laser background spontaneous emission is filtered down to a level below −110 dBm. The generated signal inside the resonator is filtered from the co-propagating pump and idler beams by using two cascaded Dense Wavelength Division Multiplexing (DWDM) modules, and directed to a photon counter (ID Quantique ID220) operating in Free Running mode, with a detection efficiency of 5% and a dead time of 40 μs. The DWDM modules achieve a signal isolation of more than 100 dB.

As discussed in Section IV, the determination of the nonlinear refractive index requires the knowledge of the extrinsic and of the total quality factors of the pump, the signal and the idler resonances. These have been extracted by measuring simultaneously the intensity and the phase of the light transmitted from the resonator as a function of wavelength. The latter has been probed by placing the sample into one arm of a free space Mach-Zehnder interferometer, as it is sketched in Fig. 1(d). For this measurement, we implemented only one C-band tunable laser, whose polarization was set at the input by a three-paddle polarization controller. The light was in and out coupled to the input/output waveguide by using two microscope objectives. The Mach-Zehnder was set in a nearly balanced regime (both in amplitude and phase) by using a delay line and a variable optical attenuator placed in the free arm. Three output signals were recorded at the output of the interferometer, which are the light transmitted from the sample I_s (when the light in the free arm is blocked), the one coming from the free arm I_{ref} (when the light in the arm which contains the sample is blocked), and their interference I. The phase is than retrieved by the relation $\phi = \arccos\left(\frac{I - I_s - I_{ref}}{2\sqrt{I_s I_{ref}}}\right)$.[21]

III. DETERMINATION OF THE THERMO-OPTIC COEFFICIENT

The thermo-optic coefficient has been measured by evaluating the resonance shift $\Delta\lambda$ as a function of the temperature variation ΔT with respect to a reference temperature of T = 28 °C. The temperature variation changes the effective index by a quantity $\Delta n_{eff}(\Delta T)$, so that each resonance gets shifted from the "cold" wavelength λ_0 by:

$$\Delta\lambda(\Delta T) = \frac{\Delta n_{eff}(\Delta T)}{n_{eff}(\lambda_0)}\lambda_0 \tag{1}$$

As shown in the inset of Fig. 2, the quantities λ_0 and $\Delta\lambda(\Delta T)$ can be extracted from the experiment. In the investigated range of temperatures the shift $\Delta\lambda$ is found to be linear. In order to compute the effective index shift, it is necessary to determine accurately the "cold" effective index $n_{eff}(\lambda_0)$. This has been shown to be quite difficult for resonators with a short spectral range.[22] Therefore, the effective index $n_{eff}(\lambda_0)$ has been computed by Finite Element Method (FEM) simulations. Due to the fact that the waveguide mode extends also into the cladding (the confinement factor of the fundamental TE and TM modes are 0.74 and 0.6 respectively), the quantity $\Delta n_{eff}/\Delta T$ is not directly the thermo-optic coefficient of the waveguide core material, but it contains information about the thermo-optical properties of both the cladding and of the core materials.

In order to decouple the two contributions, the quantity $\Delta n_{eff}/\Delta T$ is computed by FEM simulations as a function of the thermo-optic coefficient of only the bulk material Γ_{SiON}, while the refractive index of the oxide cladding n_{ox} is modelled as $n_{ox}(\Delta T) = n_{ox,0} + \Gamma_{ox}\Delta T$, where $n_{ox,0}$ is a reference refractive index at $\Delta T = 0\ K$, and $\Gamma_{ox} = 0.95 \times 10^{-5}\ K^{-1}$ is the thermo-optic coefficient of the oxide,[15] which is kept fixed during the simulation. The quantity $(\Delta n_{eff}/\Delta T)_{exp}$ extracted from the experiment, is then compared to the one computed through numerical simulations, named $(\Delta n_{eff}(\Gamma_{SiON}, \Gamma_{ox})/\Delta T)_{theo}$. The best estimate of the thermo-optic coefficient of SiON is assumed to be the value of Γ_{SiON} which matches the experimental result.

Fig. 2 reports the quantity $(\Delta n_{eff}/\Delta T)_{theo}$ as a function of Γ_{SiON} (black squares), together with $(\Delta n_{eff}/\Delta T)_{exp}$ (red dot). $(\Delta n_{eff}/\Delta T)_{exp}$ matches the simulated one if $\Gamma_{SiON} = (1.84 \pm 0.17) \times 10^{-5}\ K^{-1}$. For comparison, in Fig. 2 we also indicate the thermo-optic coefficient of silica $\Gamma_{ox} = 0.95 \times 10^{-5}\ K^{-1}$
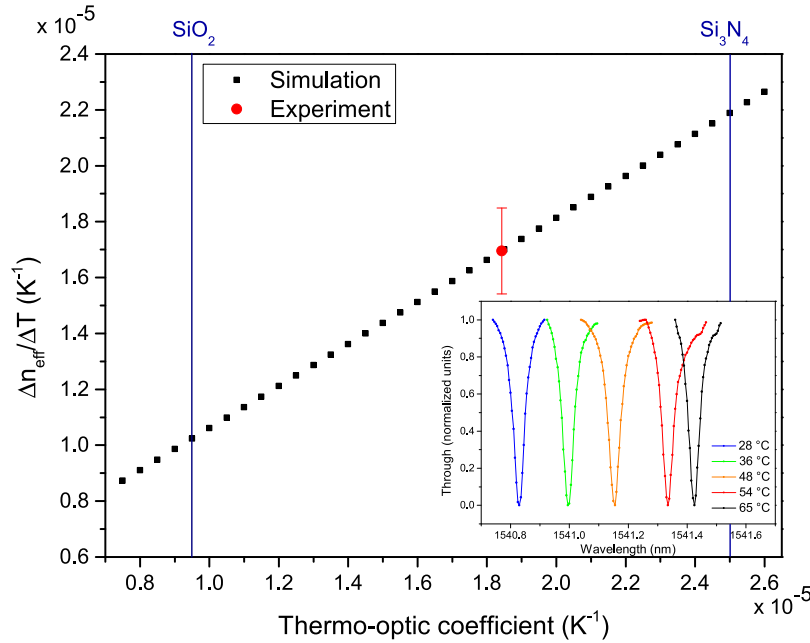
FIG. 2. Simulation of the quantity $\Delta n_{\text{eff}}/\Delta T$ as a function of the thermo-optic coefficient of the waveguide core material. The red dot shows the experimental value, which is found from the analysis of the shift of the resonance wavelength as a function of temperature (shown in the inset). The solid blue lines mark the values of the thermo-optic coefficient of silica and of stoichiometric silicon nitride reported in Ref. 15.

and the one of stoichiometric silicon nitride $\Gamma_{\text{Si}_3\text{N}_4} = 2.5 \times 10^{-5}\,K^{-1}$, both reported in Ref. 15. We point out that these values depend on the fabrication procedure, so they have to be only considered as indicative guidelines for the reader. The thermo-optic coefficient of SiON is approximately the 74% of the one of Si_3N_4.

Note that the simulation in Fig. 2 does not take into account the impact of the photoelastic effective index shift due to the accumulated stress in the waveguide, as a consequence of the temperature variation. This is however a reasonable approximation, as we estimated with a FEM simulation a maximum average stress (compressive and biaxial) of only 30 MPa in the waveguide core at 65 °C. By assuming as a first approximation the same stress-optical coefficients of stoichiometric Silicon Nitride for the Silicon Oxinitride core,[23] this leads to a photoelastic effective index shift of $3.47 \times 10^{-7}\,K^{-1}$. This value is actually two orders of magnitude lower than the one induced by the thermo-optic effect, and thus can be safely included within the error bar of our measurement.

IV. DETERMINATION OF THE NONLINEAR REFRACTIVE INDEX

The nonlinear refractive index is determined from the efficiency η of stimulated FWM. This quantity is defined as the ratio between the power of the converted signal P_s and the one of the stimulating idler P_i, and depends on the power enhancement factors $|FE(\omega_j)|^2$ (here, $j = p, s, i$ labels the pump, the signal and the idler frequency respectively) and the nonlinear coefficient γ_{nl} as:[6]

$$\eta = (\gamma_{\text{nl}}LP_p)^2|FE(\omega_p)|^4|FE(\omega_s)|^2|FE(\omega_i)|^2 \tag{2}$$

in which L is the resonator perimeter and P_p is the pump power in the waveguide. The nonlinear refractive index n_2 appears in the definition of γ_{nl} as:[6]

$$\gamma_{\text{nl}} = \frac{\omega_p n_2 n_g^2}{c n_{\text{SiON}}^2 A_{\text{eff}}} \tag{3}$$

where c is the speed of light, n_g is the group index, n_{SiON} is the bulk refractive index and A_{eff} is the effective area, defined as in Ref. 24.
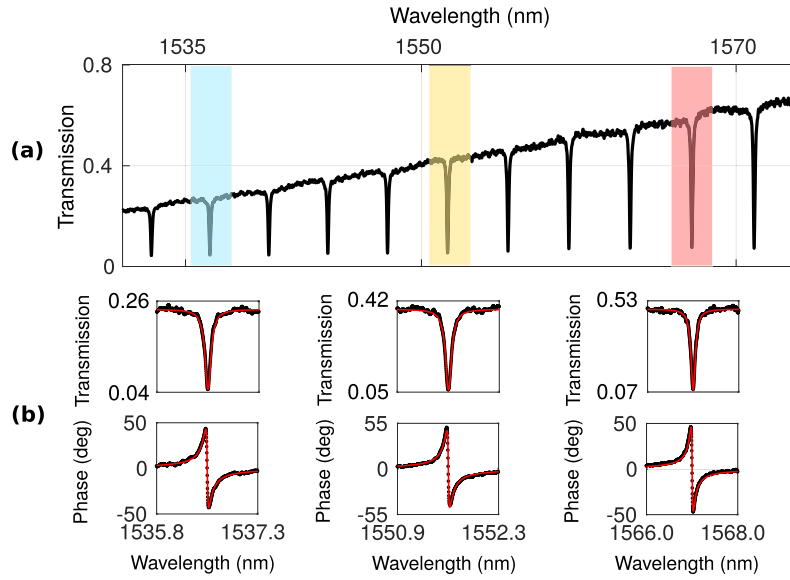
FIG. 3. (a) Normalized transmission of the resonator, with the polarization set to TM. The signal (blue), pump (yellow) and idler (red) resonance orders involved in the FWM process are highlighted with different colors. (b) Measured (black) and simulated (red) intensity and phase of the light transmitted. From left to right, the panels refer respectively to the signal, the pump and idler resonance orders.

Stimulated FWM is performed by tuning the pump and the idler laser frequencies ω_p and ω_i into two resonances orders of the resonator, shown in Fig. 3(a), and by monitoring the generated signal power at the frequency $\omega_s = 2\omega_p - \omega_i$. Since the group velocity dispersion of the implemented waveguides is non-zero at the pump wavelength, the converted signal frequency ω_s does not match perfectly the eigenfrequency ω_{0s} of the resonator, but has a normalized detuning $\delta = \frac{\omega_{0s} - \omega_s}{\omega_{0s}}$. From the simultaneous fit of the intensity and of the phase of the light transmitted from the resonator, shown in Fig. 3, the total and the extrinsic quality factors Q_{tot} and Q_{ext} have been extracted. The information carried by the phase is crucial for determining the extrinsic and the intrinsic quality factors, since their values can be exchanged without affecting the resonance linewidth and extinction ratio, which are the only quantities that can be extracted from a measurement of the intensity. As shown in Fig. 3(b), for all the three wavelengths involved in the FWM process, the phase jump across the resonance is always less than π, indicating that the resonator is undercoupled. The extrinsic quality factor must then be higher than the intrinsic one. Once Q_{tot} and Q_{ext} have been determined, the field enhancements can be computed from the relation:

$$|FE(\delta)|^2 = \frac{(\omega_0 \tau_{\text{rt}} Q_{\text{ext}})^{-1}}{\delta^2 + \left(\frac{1}{2Q_{\text{tot}}}\right)^2} \tag{4}$$

where $\tau_{\text{rt}} = L n_g / c$ is the roundtrip time of light within the cavity (n_g can be extracted from the measurement of the resonator free spectral range FSR through the relation $n_g = \frac{\lambda^2}{L \text{FSR}}$). Eq. 4 can be readily derived using temporal coupled mode theory.[25] These quantities are reported in Table I for the TE and TM polarization.

The on chip power has been estimated from the measurement of the power before entering into the chip, and from the knowledge of the propagation and coupling losses. Finally, Eq. 2 and Eq. 3 have been used to extract the value of n_2. Table II summarizes all these quantities.

The value of n_2 results to be $(6 \pm 1) \times 10^{-16}\text{cm}^2\text{W}^{-1}$ for the TE polarization, and $(8 \pm 1) \times 10^{-16}\text{cm}^2\text{W}^{-1}$ for the TM one. As expected, these values present a clear match due to the isotropic behaviour of the SiON amorphous structure.

Moreover, this value lies between the nonlinear refractive index of silica[26] ($n_2 \sim 2.36 \times 10^{-16}\text{cm}^2\text{W}^{-1}$) and the one of stoichiometric silicon nitride[27] ($n_2 \sim 2.4 \times 10^{-15}\text{cm}^2\text{W}^{-1}$). Let us state that by performing the same calculations which led to the results in Table II, but by

TABLE I. Measured resonance wavelength λ_0, total quality factor Q_{tot}, extrinsic quality factor Q_{ext}, normalized detuning δ, roundtrip time τ_{rt} and field enhancement $|FE|$ relative to the pump, the idler and the signal TE and TM resonances.

Parameter	pump (TE)	idler (TE)	signal (TE)	pump (TM)	idler (TM)	signal (TM)
λ_0 (nm)	(1551.940 ± 0.001)	(1567.045 ± 0.001)	(1537.145 ± 0.001)	(1551.590 ± 0.001)	(1566.960 ± 0.001)	(1536.540 ± 0.001)
$Q_{tot} \times 10^4$	(3.00 ± 0.04)	(2.60 ± 0.04)	(2.71 ± 0.05)	(1.50 ± 0.02)	(1.33 ± 0.01)	(1.58 ± 0.01)
$Q_{ext} \times 10^4$	(7.17 ± 0.04)	(6.53 ± 0.05)	(8.58 ± 0.07)	(3.58 ± 0.02)	(3.19 ± 0.01)	(4.30 ± 0.02)
$\delta \times 10^{-5}$	~ 0	~ 0	(1.02 ± 0.05)	~ 0	(1.96 ± 0.06)	
τ_{rt} (ps)		(2.14 ± 0.05)			(2.10 ± 0.05)	
$|FE|^2$	(19.4 ± 0.7)	(16.1 ± 0.7)	(8.4 ± 0.4)	(9.8 ± 0.3)	(8.8 ± 0.2)	(6.1 ± 0.1)

TABLE II. List of the main parameters which appear in Eq. 2 and Eq. 3.

Parameter	TE polarization	TM polarization
P_s (dBm)	(−93.80 ± 0.03)	(−98.43 ± 0.08)
P_p (dBm)	(0.5 ± 0.2)	(5.5 ± 0.2)
P_i (dBm)	(−0.6 ± 0.2)	(−3.3 ± 0.2)
Loss (dBcm^{-1})	(4 ± 0.5) (at λ_s) / (2.0 ± 0.5) (at λ_i, λ_p)	
C. loss (dBcm^{-1})	(3.0 ± 0.2)	(3.0 ± 0.2)
A_{eff} (μm^2)	0.99	1.58
γ_{nl} (m^{-1}W^{-1})	(0.25 ± 0.04)	(0.21 ± 0.03)
n_2 ($\times 10^{-16}$cm^{2}W^{-1})	(6 ± 1)	(8 ± 1)
χ^3 ($\times 10^{-22}$m^2 V^{-2})	(7 ± 1)	(9 ± 1)

considering a non-vanishing nonlinearity in the cladding region, the value of n_2 still lies within the bounds set by the experimental error. On average, the nonlinear refractive index of SiON is approximately three times larger than the one of SiO_2, and the 29.1% of the one of Si_3N_4.

V. CONCLUSIONS

In this work, an experimental characterization of the thermo-optic coefficient and of the nonlinear refractive index of silicon oxynitride waveguides has been performed. The thermo-optic coefficient results to be $\frac{dn}{dT} = (1.84 \pm 0.17) \times 10^{-5}$ K^{-1}, close to the one of stoichiometric silicon nitride. The average nonlinear parameter n_2 results to be isotropic and equal to $n_2 = (7 \pm 1) \times 10^{-16}$ cm^{2}W^{-1}, which is almost a factor of three larger with respect to the one of silica.

In addition to the well known appealing properties of the SiON, such as low insertion and propagation losses, wide transparency window from the visible to the infrared, lack of multi-photon absorption effects, CMOS compatibility and stress-free fabrication, in this paper we evaluated a sizable thermo-optic coefficient and nonlinear refractive index. The result reported here envisages that SiON has thermal and nonlinear optical properties which are competing to the other silica or silicon based materials. Hence, SiON is an excellent trade-off platform for the design of nonlinear and quantum optical integrated photonic circuits, in which thermal reconfiguration and nonlinear parametric processes constitutes fundamental operations.

[1] D. Huber, M. Reindl, Y. Huo, H. Huang, J. S. Wildmann, O. G. Schmidt, A. Rastelli, and R. Trotta, "Highly indistinguishable and strongly entangled photons from symmetric GaAs quantum dots," arXiv preprint arXiv:1610.06889 (2016).
[2] M. G. Dutt, L. Childress, L. Jiang, E. Togan, J. Maze, F. Jelezko, A. Zibrov, P. Hemmer, and M. Lukin, "Quantum register based on individual electronic and nuclear spin qubits in diamond," Science **316**, 1312–1316 (2007).

[3] J. W. Silverstone, D. Bonneau, K. Ohira, N. Suzuki, H. Yoshida, N. Iizuka, M. Ezaki, C. M. Natarajan, M. G. Tanner, R. H. Hadfield *et al.*, "On-chip quantum interference between silicon photon-pair sources," Nature Photonics **8**, 104–108 (2014).

[4] Y. Shen, N. C. Harris, S. Skirlo, D. Englund, and M. Soljačić, "Deep learning with coherent nanophotonic circuits," in *Photonics Society Summer Topical Meeting Series (SUM), 2017 IEEE* (IEEE, 2017) pp. 189–190.

[5] S. Paesani, A. A. Gentile, R. Santagati, J. Wang, N. Wiebe, D. P. Tew, J. L. O'Brien, and M. G. Thompson, "Experimental Bayesian quantum phase estimation on a silicon photonic chip," Physical Review Letters **118**, 100503 (2017).

[6] M. Borghi, C. Castellan, S. Signorini, A. Trenti, and L. Pavesi, "Nonlinear silicon photonics," Journal of Optics **19** (2017).

[7] C. Castellan, A. Trenti, M. Mancinelli, A. Marchesini, M. Ghulinyan, G. Pucker, and L. Pavesi, "From shg to mid-infrared spdc generation in strained silicon waveguides," in *Quantum Photonic Devices*, Vol. 10358 (International Society for Optics and Photonics, 2017) p. 1035804.

[8] N. C. Harris, G. R. Steinbrecher, M. Prabhu, Y. Lahini, J. Mower, D. Bunandar, C. Chen, F. N. Wong, T. Baehr-Jones, M. Hochberg *et al.*, "Quantum transport simulations in a programmable nanophotonic processor," Nature Photonics **11**, 447–452 (2017).

[9] M. Mancinelli, A. Trenti, S. Piccione, G. Fontana, J. S. Dam, P. Tidemand-Lichtenberg, C. Pedersen, and L. Pavesi, "Mid-infrared coincidence measurements on twin photons at room temperature," Nature Communications **8**, 15184 (2017).

[10] A. D. Ludlow, M. M. Boyd, J. Ye, E. Peik, and P. O. Schmidt, "Optical atomic clocks," Reviews of Modern Physics **87**, 637 (2015).

[11] A. Gondarenko, J. S. Levy, and M. Lipson, "High confinement micron-scale silicon nitride high Q ring resonator," Optics Express **17**, 11366–11370 (2009).

[12] M. Kues, C. Reimer, P. Roztocki, L. R. Cortés, S. Sciara, B. Wetzel, Y. Zhang, A. Cino, S. T. Chu, B. E. Little *et al.*, "On-chip generation of high-dimensional entangled quantum states and their coherent control," Nature **546**, 622–626 (2017).

[13] M. Fadel, M. Bülters, M. Niemand, E. Voges, and P. M. Krummrich, "Low-loss and low-birefringence high-contrast silicon-oxynitride waveguides for optical communication," Journal of Lightwave Technology **27**, 698–705 (2009).

[14] D. J. Moss, R. Morandotti, A. L. Gaeta, and M. Lipson, "New CMOS-compatible platforms based on silicon nitride and hydex for nonlinear optics," Nature Photonics **7**, 597–607 (2013).

[15] A. Arbabi and L. L. Goddard, "Measurements of the refractive indices and thermo-optic coefficients of Si_3N_4 and SIO_x using microring resonances," Optics Letters **38**, 3878–3881 (2013).

[16] J. M. Jewell, "Thermooptic coefficients of some standard reference material glasses," Journal of the American Ceramic Society **74**, 1689–1691 (1991).

[17] K. Luke, A. Dutt, C. B. Poitras, and M. Lipson, "Overcoming Si_3N_4 film stress limitations for high quality factor ring resonators," Optics Express **21**, 22829–22833 (2013).

[18] L. Stefan, M. Bernard, R. Guider, G. Pucker, L. Pavesi, and M. Ghulinyan, "Ultra-high-Q thin-silicon nitride strip-loaded ring resonators," Optics Letters **40**, 3316–3319 (2015).

[19] M. Masi, R. Orobtchouk, G. Fan, J.-M. Fedeli, and L. Pavesi, "Towards a realistic modelling of ultra-compact racetrack resonators," Journal of Lightwave Technology **28**, 3233–3242 (2010).

[20] D. E. Bossi, J. M. Hammer, and J. M. Shaw, "Optical properties of silicon oxynitride dielectric waveguides," Applied Optics **26**, 609–611 (1987).

[21] P.-É. Larré, S. Biasi, F. Ramiro-Manzano, L. Pavesi, and I. Carusotto, "Pump-and-probe optical transmission phase shift as a quantitative probe of the Bogoliubov dispersion relation in a nonlinear channel waveguide," The European Physical Journal D **71**, 146 (2017).

[22] S. Dwivedi, A. Ruocco, M. Vanslembrouck, T. Spuesens, P. Bienstman, P. Dumon, T. Van Vaerenbergh, and W. Bogaerts, "Experimental extraction of effective refractive index and thermo-optic coefficients of silicon-on-insulator waveguides using interferometers," Journal of Lightwave Technology **33**, 4471–4477 (2015).

[23] T. Capelle, Y. Tsaturyan, A. Barg, and A. Schliesser, "Polarimetric analysis of stress anisotropy in nanomechanical silicon nitride resonators," Applied Physics Letters **110**, 181106 (2017).

[24] G. P. Agrawal, *Nonlinear fiber optics* (Academic press, 2007).

[25] T. J. A. Kippenberg, *Nonlinear optics in ultra-high-Q whispering-gallery optical microcavities* (California Institute of Technology, 2004).

[26] K. Kim, W. Reed, K. Quoi, and R. Stolen, "Measurement of the nonlinear index of silica-core and dispersion-shifted fibers," Optics Letters **19**, 257–259 (1994).

[27] K. Ikeda, R. E. Saperstein, N. Alic, and Y. Fainman, "Thermal and Kerr nonlinear properties of plasma-deposited silicon nitride/silicon dioxide waveguides," Optics Express **16**, 12987–12994 (2008).